Nucleic Acids Research, 2025, **53**, gkaf219
https://doi.org/10.1093/nar/gkaf219
Chemical Biology and Nucleic Acid Chemistry

Exploring the relationship between aptamer binding thermodynamics, affinity, and specificity

Obtin Alkhamis, Caleb Byrd, Juan Canoura, Adara Bacon, Ransom Hill, Yi Xiao *

Department of Chemistry, North Carolina State University, 2620 Yarbrough Drive, Raleigh, NC 27695, United States
*To whom correspondence should be addressed. Email: yxiao34@ncsu.edu

Abstract

Aptamers are oligonucleotide-based bioreceptors that are selected *in vitro* from randomized libraries to bind specific molecules with high affinity, and are proving popular for applications in diagnostics, bioimaging, and therapeutics. A better understanding of aptamer–ligand interactions could facilitate sequence engineering efforts to improve aptamer binding properties, and perhaps eventually allow for the direct design of high-quality aptamers. To date, however, there have been very few comprehensive studies exploring the relationship between aptamer binding properties and thermodynamics. Isothermal titration calorimetry (ITC) is a gold-standard method for studying the thermodynamics of ligand–receptor interactions. In this work, we have compiled ITC-derived thermodynamic binding data from 317 small-molecule-binding DNA aptamers, along with specificity profiles for ∼6000 aptamer–ligand pairs, and performed systematic analysis of the resulting datasets. This analysis revealed a variety of interesting patterns and trends. For example, ligand binding for most aptamers is generally driven solely by enthalpy, and aptamers with the highest binding enthalpy and greatest entropic binding penalties consistently have high specificity. We envision that the expansion and further analysis of such datasets will yield a far better understanding of the complex interplay between the various non-covalent interactions underlying aptamer–ligand recognition.

Graphical abstract

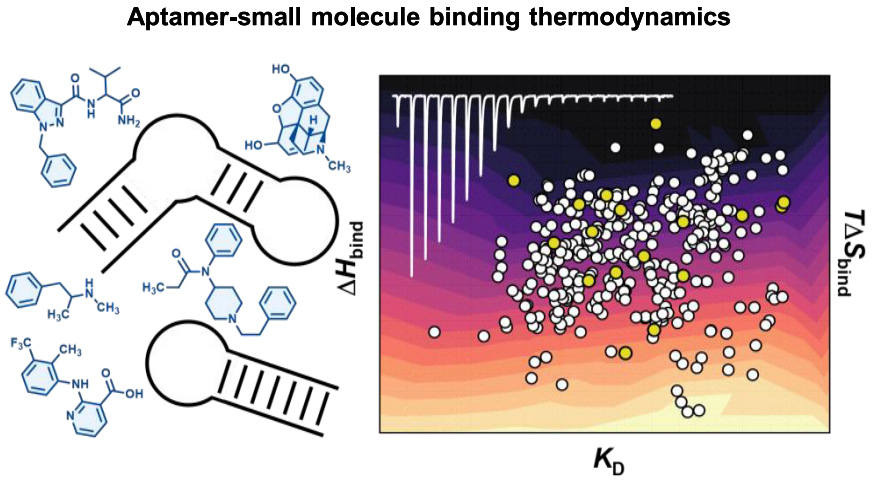

Introduction

Aptamers are short nucleic acids that bind to specific targets such as ions, small molecules, and proteins with high affinity. They are discovered from randomized oligonucleotide libraries through *in vitro* selection methods such as systematic evolution of ligands by exponential enrichment (SELEX) [1, 2]. Aptamers have generated considerable interest as receptors for biosensing and therapeutic applications due to favorable properties including faster discovery relative to antibodies, low cost of synthesis, minimal batch-to-batch variation, high stability, and amenability to chemical modification [3, 4]. More recently, advances in aptamer technology have enabled new applications that surpass the capabilities of conventional bioreceptors such as antibodies and enzymes, including high-precision continuous monitoring of circulating molecular concentrations in living organisms [5], the reversible inhibition or modulation of therapeutic protein targets [6], and controlled drug delivery [7].

The merits of aptamers notwithstanding, the fundamental basis of how aptamers interact with their targets remains

Received: November 30, 2024. **Revised:** February 18, 2025. **Editorial Decision:** March 4, 2025. **Accepted:** March 11, 2025

largely unexplored and is under active investigation. Insight into the fundamentals of aptamer–ligand binding will be crucial in terms of enabling the manipulation of aptamer–ligand interactions through sequence engineering—and eventually, the *de novo* construction of aptamers without the need for tedious *in vitro* selection. Three-dimensional structures of aptamer–ligand complexes obtained through X-ray crystallography and nuclear magnetic resonance spectroscopy have revealed that aptamers interact with ligands through a variety of intermolecular forces including electrostatics, dipole interactions, hydrogen bonding, pi stacking, and hydrophobic interactions [8–13]. Despite these valuable insights, the number of solved three-dimensional aptamer structures is small relative to the vast number of aptamers reported in the literature. As an alternative, most investigators have relied on cruder but still informative biophysical methods to characterize aptamer-target binding. One of the most well-established approaches is isothermal titration calorimetry (ITC), which can reveal the binding enthalpy, entropy, and stoichiometry between aptamers and ligands [14] and provide other insights including the nature of hydrophobic interactions and conformational changes via changes in solution heat capacity [15, 16]. ITC and other methods like surface plasmon resonance [17] and strand-displacement assays [18] have proven useful for verifying the binding properties of aptamers [19–21], and have also served as a tool to understand aptamer–ligand structure–affinity relationships [22–27]. Nevertheless, there have been very few systematic, comprehensive studies [19, 28–31] conducted to unravel the complex interplay between the thermodynamics of aptamer binding and aptamer affinity and specificity, especially with an expansive set of diverse aptamer–ligand pairs. In analogy to medicinal chemistry, where the structure and functional groups of small molecules are tuned to maximize receptor binding affinity (and hence biological potency), we propose that thermodynamic data could aid in achieving a similar goal in the aptamer field – the optimization of aptameric receptors via mutagenesis or chemical modification, with the guidance of biophysical data, to maximize ligand affinity and specificity.

To this end, we have compiled and analyzed ITC affinity data for 317 small-molecule-binding DNA aptamers and specificity profiles from an exonuclease-based assay [32] for ~6000 aptamer–ligand pairs. Our specificity data were derived from a panel of 218 different aptamers with diverse sequence composition and secondary structures, assessing their binding to 18–35 different small-molecule ligands of varying size, shape, polarity, and hydrophobicity. Overall, we find that the relationship between aptamer binding thermodynamics and binding properties is nuanced and varied. We have also identified several interesting patterns in these data. First, unlike the interaction between proteins and small molecules, which is in many cases enthalpically and entropically favorable [33, 34], aptamer–ligand binding is predominantly an enthalpy-driven, entropically unfavorable phenomenon. Second, aptamers with the most negative binding enthalpies and entropies do not have higher affinity; instead, aptamers with moderate binding enthalpies and entropies tend to have the highest affinity. Third, aptamers with very negative binding enthalpy and entropy have a high likelihood of being specific. We see this work as an important starting point in a broader effort to explore the influence of thermodynamic properties on aptamer affinity and specificity, thereby advancing the field's progress toward the ability to rationally engineer aptamers for optimal target binding affinity and specificity.

Materials and methods

Oligonucleotides

All DNA oligonucleotides were purchased from Integrated DNA Technologies as standard desalted quality. Oligonucleotides were dissolved in molecular-biology-grade water, and DNA concentrations were measured using a NanoDrop 2000 spectrophotometer.

Reagents and materials

Molecular biology-grade water and 10× phosphate-buffered saline were purchased from Corning. Exonuclease I (*Escherichia coli*) and T5 Exonuclease (*E. coli*) were purchased from New England Biolabs. Bovine serum albumin (BSA), Tris base, Tris HCl, 5 M NaCl solution, 1 M $MgCl_2$ solution, potassium chloride, sodium hydroxide, Triton X-100, lactose, mannitol, lidocaine HCl, diphenhydramine HCl, procaine HCl, benzocaine, ibuprofen sodium, acetaminophen, caffeine, quinine hemisulfate hydrate, serotonin HCl, pseudoephedrine HCl, xylene cyanol, acrylamide, and bis-acrylamide were purchased from Sigma–Aldrich. Levamisole HCl was purchased from MP Biomedicals. Scopolamine hydrobromide trihydrate was purchased from Acros Organics. Nicotine, mephedrone HCl, methylenedioxypyrovalerone (MDPV) HCl, methylphenidate HCl, fentanyl HCl, (+)-methamphetamine HCl, methylenedioxymethamphetamine (MDMA) HCl, morphine sulfate hydrate, heroin HCl, amphetamine HCl, benzoylecgonine, fluoxetine HCl, and methadone HCl were purchased from Cayman Chemicals. Cocaine HCl was purchased from Cayman Chemicals and Sigma–Aldrich. Formamide was purchased from Fisher Scientific.

Molecular properties of small molecules

The physicochemical properties of the small-molecule targets in this work were determined or predicted using the ChemDraw software (v18.2).

ITC

All ITC experiments were performed at 23°C in each aptamer's respective selection buffer (Supplementary Table S1) using a Malvern MicroCal iTC200 or PEAQ-ITC instrument. Solutions containing ligand or aptamer at various concentrations were prepared and respectively loaded into the instrument pipet and cell. The aptamer was initially snap-cooled in salt-free buffer, after which salts were added to the final appropriate concentration. After a 60-s delay to establish a baseline reading, an initial 0.4-µl purge injection was performed, followed by 19 successive 2-µl injections. Spacing between each injection was typically 150 s, but was adjusted for certain titration experiments (up to 1200 s) due to slow equilibration. If saturation of the aptamer was not achieved, another series of titrations was performed by refilling the syringe with ligand and titrating the aptamer solution into the cell again. The resulting data were analyzed using the MicroCal analysis kit that comes with the instrument with a one-site binding model. For all ITC data, c-values were >1. Approximately 20% of the ITC data was replicated twice, and a standard deviation < 20% was observed in ΔH_{bind} and K_D.

Screening aptamer specificity via exonuclease digestion assay

The exonuclease digestion fluorescence assay was performed as described previously [32, 35]. Each aptamer (final concentration: 0.5 or 1 μM) was diluted into the appropriate buffer, heated to 95°C for 10 min, and then immediately cooled on ice. Salts including NaCl, $MgCl_2$, and BSA (final concentration: 0.1 mg/ml) were then added. In brief, 5 μl of the aptamer solution was mixed with 20 μl of buffer alone or target/interferent dissolved in buffer at various concentrations. These mixtures were incubated at 25°C for 30 min, after which 25 μl of exonuclease mixture was added (T5 and Exo I, final concentrations: 0.2 and 0.015 U/μl, respectively) in buffer containing 0.1 mg/ml BSA to begin the digestion. Then, 5 μl of sample was collected at various timepoints and mixed with 30 μl of quenching solution in the wells of a 384-well black microplate. Quenching solution contained 10 mM Tris–HCl (pH 7.4), 21 mM ethylenediaminetetraacetic acid, 12.5% (v/v) formamide, and 1× SYBR Gold (final concentrations). SYBR Gold fluorescence was recorded using a Tecan Spark plate reader with an excitation wavelength of 495 nm and emission wavelength of 537 nm. The fluorescence of each sample was recorded 10 times, and average values were used to construct time-course digestion plots of each sample. The integration time was customized for each aptamer, and was chosen as the point at which fluorescence reached 10% of its initial value. Enzymatic inhibition was measured in terms of resistance value, as described previously [32]. Resistance values were used to calculate the cross-reactivity of each interferent relative to the target of the aptamer. Specificity scores were calculated by taking the average cross-reactivity of all nontarget molecules tested for that particular aptamer (see "Aptamer Specificity Score Excel File" for details).

Results

An overview of the constituents in the thermodynamic dataset

All 317 aptamers in our dataset are DNA-based and were discovered from various library-immobilized SELEX campaigns as well as two nuclease-assisted SELEX experiments performed by our group in the past half decade (Supplementary Tables S2–S12 for sequences) [35–46]. The overall sequence composition of these aptamers is somewhat biased toward G and T nucleobases relative to A and C, which likely originates from the G and T bias observed with the oligonucleotide libraries that we used for the selection of these aptamers [43, 47]. Since these aptamers were discovered from stem-loop structured libraries, they all contain an initial 8-bp stem that is pre-folded at room temperature (T_m = 41 – 62°C depending on the stem composition of the library according to NUPACK [48]) and an internal loop, which was 30 nucleotides (nt) in most cases but 40 nt for some aptamers serving as the target-binding domain. We assume that these binding domains form complex, noncanonical structures. But as the tertiary structures of these aptamers have not yet been determined, we can only obtain a basic picture of their folding using structure-prediction software such as NUPACK [48] and mfold [49]. Both methods indicate the presence of a variety of structures within the loop domain, such as bulges, internal hairpins, cruciforms, and three-way junctions (Supplementary Figs S1–S12). The majority of these aptamers were selected against 15 different small-molecule targets, with moderate variety in terms of molecular weight (149–378 Da) but broad diversity in terms of structure, number of rotatable bonds (0–10), number of hydrogen bond donors (0–3) and acceptors (1–7), polar surface area (12–87.8 $Å^2$), hydrophobicity (LogP = 0.4–5.5), and charge (Table 1). For example, our smallest ligand, methamphetamine (149 Da), is moderately hydrophobic (LogP = 2.2) and has the fewest heavy atoms (11) and rotatable bonds (3) among our ligands, with a positive charge at pH 7.4. In contrast, one of our bulkiest ligands, the synthetic cannabinoid 5F-AMB (379 Da), is neutral in charge, has the second-most heavy atoms (27) and most rotatable bonds (10), and is among the most hydrophobic molecules in our dataset (LogP = 3.6) except for the natural cannabinoid Δ^9-tetrahydrocannabinol (THC) (LogP = 5.5).

The relationship between aptamer binding thermodynamics and affinity

The binding between an aptamer and a small-molecule ligand can be modeled as a reversible reaction wherein the two species associate to form a receptor–ligand complex. The equilibrium constant of the reverse of this process (K_D)—the dissociation of the complex into free aptamer and ligand—is a useful metric to quantify affinity. When the affinity between the aptamer and ligand is high, the K_D is small, whereas the K_D increases as affinity weakens. ITC can provide a direct measurement of K_D—and by extension, the free energy of binding, ΔG_{bind}—through the equation $\Delta G = RTln(K_D)$, as well as the enthalpy of binding (ΔH_{bind}) and binding stoichiometry (n). The entropy of binding (ΔS_{bind}), however, must be calculated indirectly using the equation $\Delta G = \Delta H - T\Delta S$.

We performed ITC and determined K_D, ΔH_{bind}, and ΔS_{bind} for 319 aptamer–ligand pairs (Supplementary Tables S13–S23). Examining the thermodynamic data superficially, we found that these values varied widely, with ranges of K_D = 4–27 400 nM, ΔH_{bind} = −43.0 – −3.5 kcal/mol, and $T\Delta S_{bind}$ = −35.4 – 3.2 kcal/mol (Fig. 1A). We first determined whether there was a relationship between binding enthalpy and affinity by plotting ΔH_{bind} for each aptamer–ligand pair against K_D, and saw no correlation between these two parameters (Fig. 1B). This is not completely surprising; the main contributor to binding enthalpy is the formation of attractive or repulsive intermolecular forces between the target and aptamer (i.e. non-covalent bonding), such as electrostatic interactions, hydrogen bonds, and pi stacking. Intuitively, the more non-covalent bonds form between the aptamer and target, the greater the binding enthalpy, and perhaps sensibly, the stronger the affinity between the two species. However, as more bonds are formed between the aptamer and ligand, the entropy, or the disorder of the system (i.e. the rotational and translation freedom of the aptamer and ligand), decreases, reducing the overall free energy of binding and binding affinity. As such, the lack of correlation between ΔH_{bind} and K_D is reasonable. We do note, however, that this explanation neglects other events that can contribute to ΔH_{bind}, such as the formation or breakage of non-covalent bonds within the aptamer itself due to, e.g., base-pairing of nucleotides upon target binding. Unfortunately, it is challenging to decouple the enthalpic contributions from aptamer-target binding and target-induced aptamer folding. We next assessed the relationship between binding entropy and affinity by plotting $T\Delta S_{bind}$ against K_D. Once again, we observed no apparent correlation between these two pa-

Table 1. Physicochemical properties of the aptamer ligands in our dataset

Ligand	MW (Da)	Rotatable bonds	HB Donor(s)	HB Acceptor(s)	Polar SA (Å^2)	LogP	Charge @ pH 7.4	Aptamers in dataset
Cocaine	303	3	1	5	55.8	1.82	+1	71
Methamphetamine	149	3	1	1	12	2.20	+1	32
Flunixin	296	3	1	7	61.7	3.84	−1	18
5F-AMB	363	10	1	7	71	3.60	0	7
AB-FUBINACA	368	6	2	7	87.8	2.87	0	37
Heroin	369	4	1	6	65.1	1.39	+1	23
Morphine	285	0	3	4	52.9	1.19	+1	31
Oxycodone	315	1	2	5	59	0.36	+1	25
Fentanyl	336	6	1	3	23.6	3.79	+1	51
Furanyl fentanyl	375	6	1	4	32.8	3.65	+1	10
Acetyl fentanyl	322	5	1	3	23.6	3.14	+1	9
UR-144	311	6	0	2	20.3	5.10	0	2
THC	314	4	1	2	29.5	5.53	0	1
Mephedrone	177	3	1	2	29.1	1.76	+1	1
MDPV	275	5	1	4	38.8	2.65	+1	1

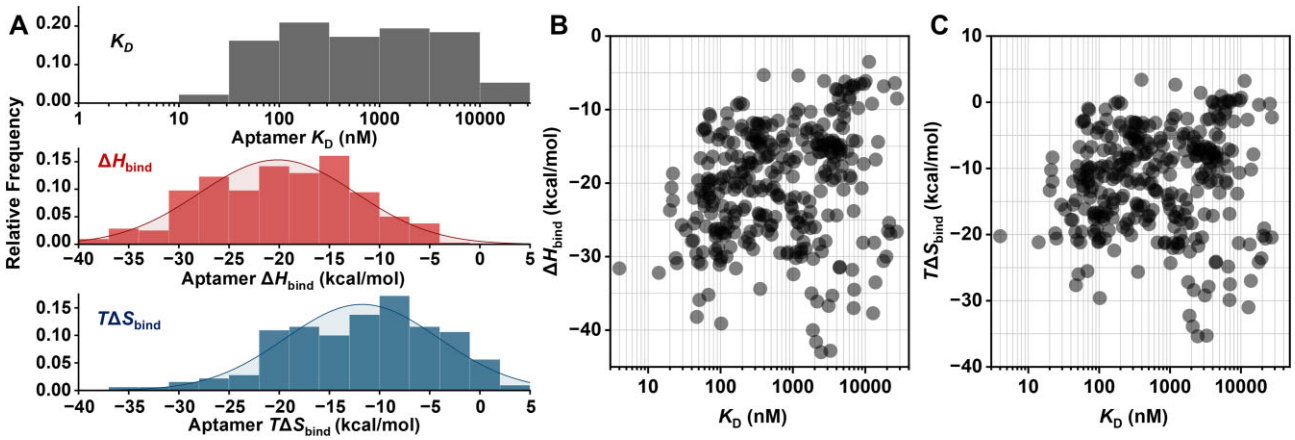

Figure 1. Binding thermodynamics of a diverse set of small-molecule-binding DNA aptamers discovered by our lab. (**A**) Histograms and distribution curves for the K_D (top panel), ΔH_{bind} (middle panel), and $T\Delta S_{bind}$ (bottom panel) of aptamers for their respective targets. The K_D for each aptamer–ligand pair is plotted against (**B**) ΔH_{bind} and (**C**) $T\Delta S_{bind}$.

rameters (Fig. 1C), which can be explained by the fact that affinity—essentially a surrogate of binding free energy—is affected by a combination of both binding entropy and enthalpy.

Binding thermodynamics and ligand structure

We next determined whether there was any correlation between the identity of the aptamer target and binding thermodynamics. Based on the diversity of target structures (Fig. 2A), we expected to see similarly variable binding thermodynamics. To assess this, we created box-and-whisker plots based on the aptamer binding thermodynamics of each target for which we had at least five different aptamers. We initially observed that the average K_D varied depending on the target (Fig. 2B). For instance, we saw the highest binding affinity among aptamers for fentanyl and its analogs acetyl fentanyl and furanyl fentanyl. The high affinity of aptamers toward these ligands is reasonable, given that they contain multiple moieties that enable tight interactions with nucleic acids. These include aromatic rings, a piperidinyl amino group that is positively charged at pH 7.4, and an amido group containing hydrogen bond donors and acceptors. However, even though heroin, oxycodone, and morphine also contain several moieties that could contribute to high-affinity recognition, aptamers tended to have much lower affinity on average for these ligands compared with fentanyl. Interestingly, this pattern of binding is reminiscent of that of the human μ-opioid receptor, which generally exhibits affinity for fentanyl that is one or two orders of magnitude higher relative to other morphine-related opioids [50]. There are two possible reasons for this difference in affinity. The first is that the bulky T-shaped structure of morphine-like opioids makes it difficult for aptamers to optimally engage all potential contact points on the target, especially if the aptamer binding domain is limited in terms of size and complexity. This is corroborated by the Stojanovic group, which has noted the difficulty of aptamers have binding to sterically crowded ligands [51]. It is also possible that certain favorable epitopes of fentanyl (i.e. aromatic rings and amino group) synergistically improve affinity; the Stojanovic group has recently begun to explore the first principles underlying these synergistic effects [51].

Aptamers for cocaine and AB-FUBINACA also tended to have relatively high affinity, albeit somewhat lower than fentanyl on average. Both ligands also feature several favorable moieties for recognition by nucleic acids, including aromatic rings and multiple hydrogen bond donors and acceptors. This is in line with recent findings by the Stojanovic group, which found that targets with amino groups and aromatic rings are more amenable to binding aptamers [51]. Aptamers for AB-FUBINACA, however, tended to have a wider range of affini-

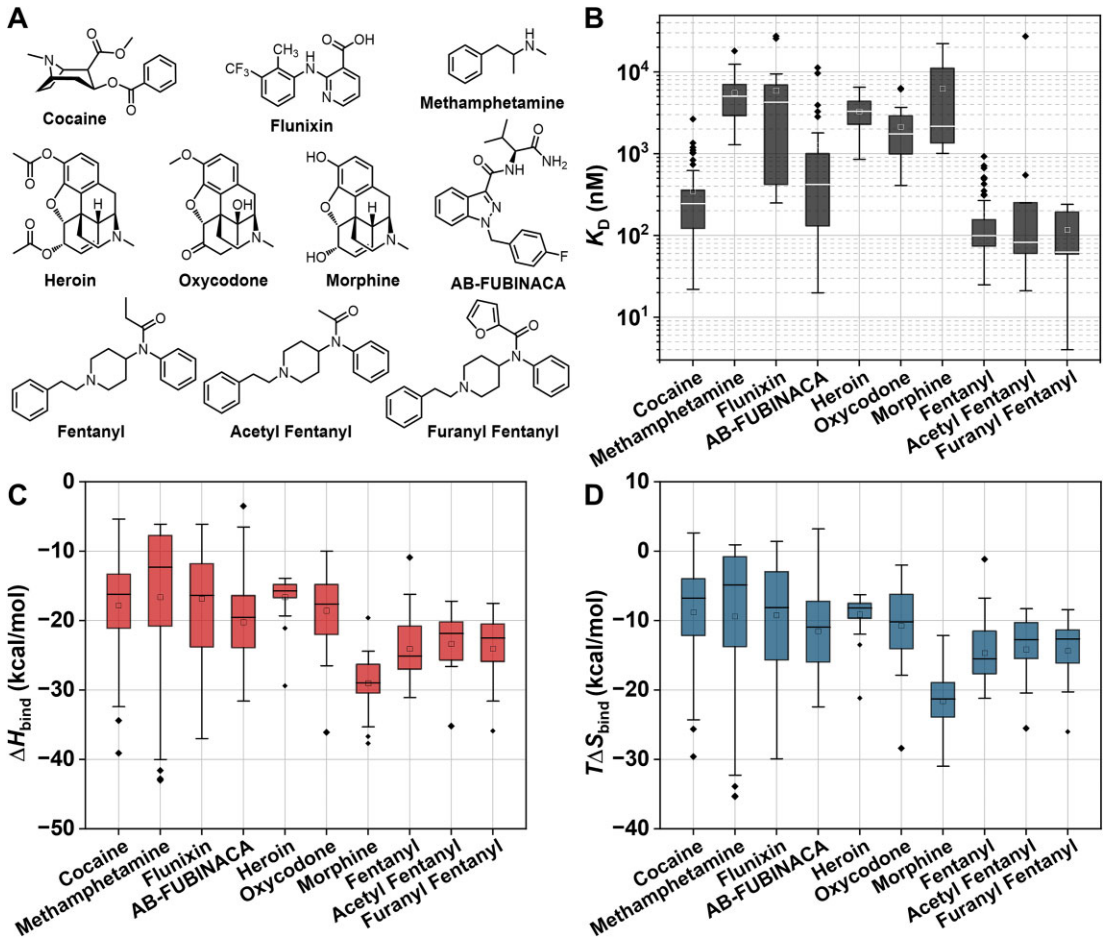

Figure 2. Assessing relationships between target structure and aptamer-ligand binding thermodynamics. (**A**) Structures for the various small-molecule targets for our aptamers. Box-and-whisker plots of aptamer (**B**) affinity, (**C**) enthalpy, and (**D**) entropy for each target.

ties, perhaps because there are more binding epitopes and combinations thereof on AB-FUBINACA that aptamers could interact with relative to cocaine. These same notions hold true for flunixin aptamers as well, which have K_Ds that span over two orders of magnitude. Aptamers for methamphetamine and flunixin had the lowest affinity, most likely because they offer smaller binding surfaces and fewer epitopes for interaction than the other ligands. We did not observe any obvious correlations in terms of binding enthalpy and entropy for each target (Fig. 2C and D), as these values varied broadly. We did, however, notice some peculiarities. In particular, the fentanyl aptamers, which had the highest affinity among all aptamers in the dataset, tended to have moderate binding enthalpies and entropies. In addition, for reasons that are unclear to us, morphine aptamers had the most negative binding enthalpies and entropies among all ligands, while those for heroin were among the least negative. Despite their ligands differing substantially in structure, we observed no meaningful difference in the range of binding enthalpy and entropy of aptamers for cocaine, methamphetamine, flunixin, and AB-FUBINACA. However, we found that for most of our ligands, aptamers that bind the same ligand can have widely varying binding enthalpies and entropies. For instance, the range of ΔH_{bind} for methamphetamine aptamers spans from −43 to −8 kcal/mol. This implies that different aptamers can bind to the same ligand with differing sets of intermolecular interactions.

The apparent balance between binding enthalpy and entropy

Having observed no meaningful correlation between ΔH_{bind} or $T\Delta S_{bind}$ and K_D, we next determined if there was a correlation between binding entropy and enthalpy by plotting $T\Delta S_{bind}$ against $\Delta H_{bind.}$ Interestingly, when we fit the entire dataset with a linear equation, we observed a near-perfect linear relationship between the two parameters (Fig. 3A), with a correlation coefficient (R^2) of 0.98. A similar correlation has previously been observed with protein transmembrane receptors and enzymes binding to small-molecule ligands. This correlation, which has been termed "enthalpy–entropy compensation" [33], describes the phenomenon wherein as binding enthalpy becomes increasingly negative, the binding entropy also becomes increasingly negative in a nearly proportional manner, and *vice versa*. Data reported by the Johnson group has revealed that enthalpy–entropy compensation also occurs with the cocaine aptamer [31], and indeed, our extensive dataset here confirms this to be true with small-molecule-binding aptamers in general. This is best evidenced by examining the binding thermodynamics of aptamers that lie precisely on the red linear fit in Fig. 3A. Aptamers on this line have identical, or very similar, target-binding affinities (in this case, K_D ~1 μM) but differing binding enthalpies and entropies. We observed similar such linear correlations among other aptamers that share other affinities—see the pink (K_D ~20 nM) and blue (K_D ~25 μM) lines in Fig. 3A—henceforth

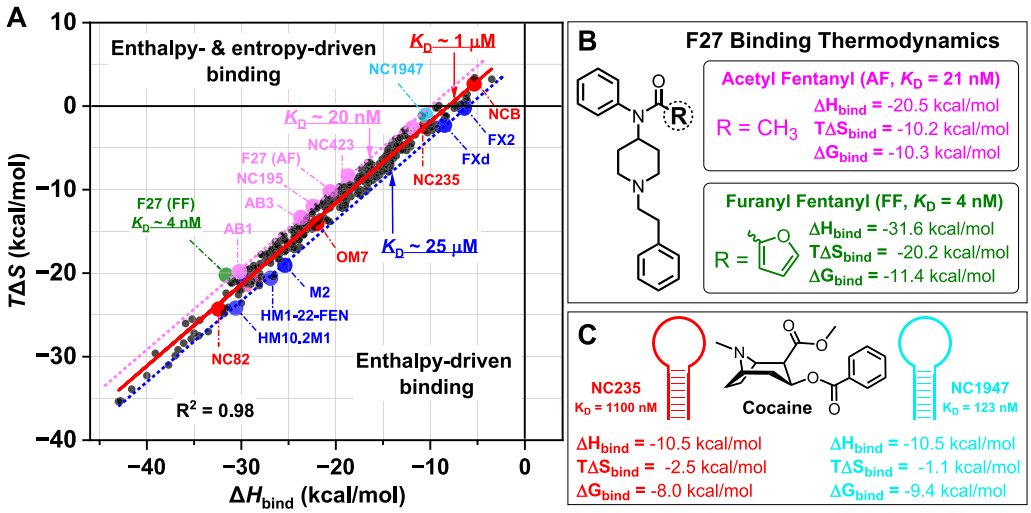

Figure 3. The relationship between aptamer binding enthalpy and entropy. (**A**) Aptamer binding enthalpy plotted against entropy for all aptamers in the dataset. The entire dataset was fitted with a linear trendline, which is indicated by a solid red line ($R^2 = 0.98$). Aptamers that lie on the line of fit have K_D of ~1 μM, and a few example aptamers are marked as red circles. Dotted pink and blue diagonal lines above or below the line of fit indicate affinity diagonals along which aptamers share roughly equivalent K_D values despite exhibiting considerably different thermodynamic properties, demonstrating the enthalpy–entropy compensation effect. Examples of such aptamers are colored accordingly. (**B**) Comparison of the binding thermodynamics of aptamer F27 to acetyl fentanyl and furanyl fentanyl. (**C**) Comparison of the binding thermodynamics of cocaine-binding aptamers NC235 and NC1947.

we refer to such lines as affinity diagonals. For example, the cocaine aptamers NCB and NC82 both fall on the ~1-μM affinity diagonal. With a K_D of 1.0 μM, NCB has a relatively small ΔH_{bind} of −5.4 kcal/mol and a slightly favorable entropy term ($T\Delta S_{bind}$ = +2.7 kcal/mol). In contrast, NC82 has a nearly six-fold greater enthalpic contribution (ΔH_{bind} = −32.4 kcal/mol) compared with NCB, but with a larger binding entropy penalty ($T\Delta S_{bind}$ = −24.3 kcal/mol) that almost completely negates any net gain in affinity (K_D = 1.4 μM). Another example is the oxycodone aptamer OM7, which has a lower entropic penalty compared with NC82 ($T\Delta S_{bind}$ = −14.1 kcal/mol) but still exhibits the same affinity for its ligand (K_D = 1.4 μM) because that entropy benefit is offset by a relatively lower enthalpic contribution (ΔH_{bind} = −22 kcal/mol). We note however that, although there appears to be a compensatory relationship between ΔH_{bind} and $T\Delta S_{bind}$, this seemingly linear relationship may be artifactual due to inaccuracies in measuring binding enthalpy [52] and the narrow range of ΔG_{bind} examined here, which is discussed in depth by Chodera and Mobley [53].

We observed similar patterns along the other affinity diagonals demarcated on our plot. For example, FX2 and FXd both bind the small molecule flunixin with near-identical affinities (K_D of 25.6 and 27.4 μM, respectively), but have markedly differing binding thermodynamics (Fig. 3A, blue diagonal). FX2 has a relatively small enthalpic binding contribution (ΔH_{bind} = −6.4 kcal/mol) with a negligible entropic contribution ($T\Delta S_{bind}$ = −0.2 kcal/mol). In contrast, FXd has a nearly 30% more favorable binding enthalpy (ΔH_{bind} = −8.5 kcal/mol), but this is offset by the increased entropic cost of binding ($T\Delta S_{bind}$ = −2.3 kcal/mol). The same enthalpy–entropy compensation effect can also be observed for aptamers binding to other ligands on this same low-affinity diagonal. For instance, morphine aptamers M2, HM1-22-FEN1, and HM10.2M1, which have similar K_Ds of 21.3, 22.0, and 17.8 μM, respectively, exhibit progressive decreases in enthalpy (ΔH_{bind} = −25.4, −26.9, and −30.6 kcal/mol, respectively) that are essentially offset by increasing entropic costs ($T\Delta S_{bind}$ = −19.1, −20.6, and −24.2 kcal/mol, respectively), thereby negating any significant improvement in affinity. Aptamers with higher affinities also obeyed the enthalpy–entropy compensation rule. For instance, AB-FUBINACA aptamer AB1 (K_D = 24 nM) features primarily enthalpy-driven binding (ΔH_{bind} = −30.2 kcal/mol, $T\Delta S_{bind}$ = −19.8 kcal/mol), whereas the binding enthalpy is only half as much (−18.7 kcal/mol) for cocaine aptamer NC423, which achieves an equally high affinity (K_D = 22 nM) through a roughly equivalent reduction in the entropic cost of binding ($T\Delta S_{bind}$ = −8.3 kcal/mol). Other aptamers on the same high-affinity diagonal (e.g. F27, NC195, and AB3) also demonstrated similar effects (Fig. 3A, pink diagonal).

Altogether, the thermodynamic data indicate that for a majority of aptamers, differences in the binding enthalpy between different aptamers are generally directly compensated for by equivalent changes in entropy, and it appears as if only aptamers that can overcome this compensation effect can achieve higher affinity. An apparent instance of this is with the aptamer F27, which binds furanyl fentanyl with very high affinity (K_D = 4 nM; labeled green in Fig. 3A). Thermodynamic data indicate that the furanyl moiety of this target is involved in binding, as the absence of this group, which results in the analog acetyl fentanyl, reduces the affinity of F27 by five-fold (K_D = 21 nM; labeled pink in Fig. 3A) and increases ΔH_{bind} by a staggering +11.0 kcal/mol. Interestingly, we calculated a $T\Delta S_{bind}$ for F27 binding to furanyl fentanyl and acetyl fentanyl of −20.2 and −10.2 kcal/mol, respectively. This means that the additional enthalpic contribution of binding to the furanyl moiety ($\Delta\Delta H_{bind}$ = −11.0 kcal/mol) overcomes the additional entropic cost ($T\Delta\Delta S_{bind}$ = −10.0 kcal/mol), thereby contributing −1.0 kcal/mol toward ΔG_{bind} —and hence the observed five-fold improvement in affinity (Fig. 3B). As another example, aptamers NC235 and NC1947 both bind cocaine with an identical ΔH_{bind} of −10.5 kcal/mol. However, NC1947 (labeled aqua in Fig. 3A) has a nearly 10-fold superior affinity relative to NC235 (labeled red) (123 versus 1100 nM) because it has less than half

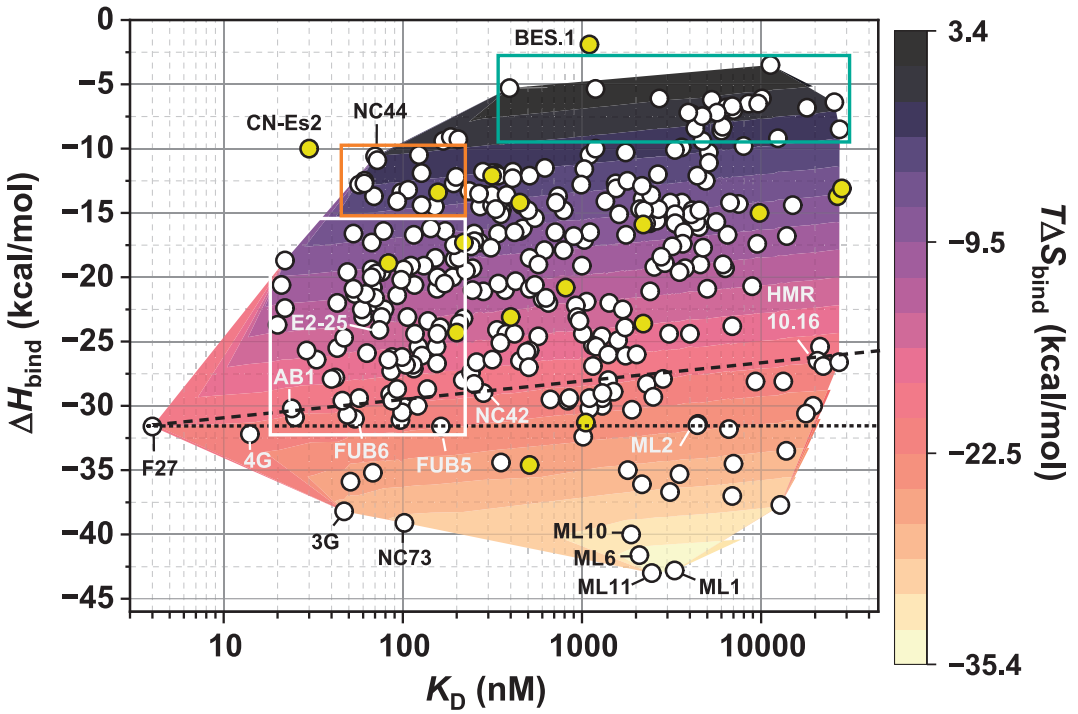

Figure 4. The relationship between aptamer K_D, enthalpy, and entropy. The binding thermodynamics of aptamers in our dataset as well as aptamers reported by other research works are marked as white and yellow circles, respectively. Aptamers specifically discussed in the manuscript are labeled. The color gradient represents binding entropy ($T\Delta S$). The dotted and dashed lines indicate aptamers that share similar binding enthalpy and entropy values as F27, respectively. Colored boxes represent groups of aptamers referred to in the manuscript.

of the entropic binding penalty ($T\Delta S_{bind}$ = −1.1 versus −2.5 kcal/mol), allowing it to similarly overcome the compensation effect (Fig. 3C).

The interplay between binding affinity, enthalpy, and entropy

To better visualize the relationship between binding enthalpy, entropy, and affinity, we created a two-dimensional contour plot where affinity and enthalpy are plotted against each other and entropy is represented as a color gradient (Fig. 4). From this plot, we can make several observations. First, we find that the highest affinity aptamer in our dataset, F27 (K_D = 4 nM), has neither the most negative binding enthalpy (ΔH_{bind} = −31.6 kcal/mol) nor the least negative binding entropy ($T\Delta S_{bind}$ = −20.2 kcal/mol)—factors that both lend themselves to high-affinity binding. To better understand why F27 has such high affinity, it is instructive to examine the binding thermodynamics of aptamers FUB6 (ΔH_{bind} = −31.0 kcal/mol), FUB5 (ΔH_{bind} = −31.6 kcal/mol), and ML2 (ΔH_{bind} = −31.4 kcal/mol), which have the same or similar binding enthalpy (Fig. 4, dotted line). However, these aptamers have affinities that are orders of magnitude poorer than that of F27 (K_D = 54, 163, and 4400 nM, respectively) because of their greater binding entropy penalties relative to F27 ($T\Delta S_{bind}$ = −21.2, −22.4, and −24.1 kcal/mol, respectively). It is also informative to examine aptamers with similar binding entropies to F27 but differing binding affinities and enthalpies—specifically, AB1 ($T\Delta S_{bind}$ = −19.8 kcal/mol, K_D = 24 nM), NC42 ($T\Delta S_{bind}$ = −20.1 kcal/mol, K_D = 282 nM), and HMR10.16 ($T\Delta S_{bind}$ = −20.2 kcal/mol, K_D = 20.6 μM) (Fig. 4, dash line). With ΔH_{bind} of −30.2, −29.0, and −26.5 kcal/mol, respectively, these aptamers all have less favorable enthalpic binding contributions than F27. Thus, F27 is capable of achieving single digit nanomolar affinity by having both favorable binding enthalpy and the smallest entropic binding penalty among these aptamers. This notably low entropic cost implies that the multiple non-covalent interactions formed between the target and aptamer are perhaps aided by more stable pre-folding of the binding site relative to other aptamers. Alternatively, this high affinity may be a consequence of the hydrophobic effect. Here, water molecules that are initially arranged in an orderly fashion around furanyl fentanyl gain more conformational freedom as furanyl fentanyl is sequestered by the aptamer and/or water molecules initially bound by the ligand-free aptamer are liberated into bulk solution upon target binding. This is a reasonable assumption given that furanyl fentanyl is fairly hydrophobic (LogP = 3.5)—more so than other ligands in our dataset.

We further observed that the aptamers with the most negative binding enthalpy tended to have lower affinity. Starting from F27 as a point of reference, as the binding enthalpy increases for aptamers 3G (ΔH_{bind} = −38.2 kcal/mol), NC73 (ΔH_{bind} = −39.1 kcal/mol), and ML10 (ΔH_{bind} = −40.0 kcal/mol), the affinity of the aptamers becomes substantially poorer, with respective K_Ds of 47 nM, 102 nM, and 1.88 μM. The reason for this reduction in affinity is the increasing entropic binding penalty ($T\Delta S_{bind}$ = −27.7, −29.6, and −32.2 kcal/mol, respectively) that is incurred as enthalpy contributions increase, which mitigates increases in overall affinity. Compared with F27, which may feature a more pre-organized binding domain, the binding sites of 3G, NC73, and ML10 may be less organized and undergo more extensive conformational changes upon target binding, resulting in a more severe entropic binding penalty. A similar phenomenon can be seen in comparing the 3G and 4G cocaine aptamers recently isolated

by the Stojanovic group [54]. Aptamer 4G (K_D = 14 nM) was selected from a library containing the 3G aptamer (K_D = 47 nM) sequence with an additional N22 random domain inserted and has ~3.5-fold higher affinity than 3G. Although the binding enthalpy for 4G (ΔH_{bind} = −32.2 kcal/mol) is less favorable than that of 3G (ΔH_{bind} = −38.2 kcal/mol), the lower entropic binding penalty for 4G ($T\Delta S_{bind}$ = −21.1 kcal/mol) relative to 3G ($T\Delta S_{bind}$ = −27.7 kcal/mol) confers higher affinity. The 22-nt insertion in 4G may result in more pre-organization and rigidity in this aptamer relative to 3G in the absence of target, thereby increasing aptamer–cocaine affinity, whereas the more negative enthalpy and entropy values for 3G may reflect greater flexibility and disorganization of this aptamer in its unbound state.

Interestingly, as binding enthalpies become more favorable (i.e. more negative ΔH_{bind}), aptamer binding affinity becomes even poorer. For example, the methamphetamine aptamers ML1, ML6, and ML11, all have $\Delta H_{bind} < -40$ kcal/mol and also have K_D values in the micromolar range (3.3, 2.1, and 2.5 μM, respectively). This is primarily because these aptamers also have the highest entropic binding penalties among all the aptamers in our dataset, with respective $T\Delta S_{bind}$ of −35.3, −33.9, and −35.4 kcal/mol. Interestingly, the overwhelming majority of high-affinity (i.e. K_D = 20–125 nM) aptamers in our dataset have moderate enthalpy contributions ranging from −32 to −15 kcal/mol (Fig. 4, white box). For example, E2-25 has a K_D of 74 nM and a ΔH_{bind} of −24.1 kcal/mol. We also identified aptamers in the ΔH_{bind} range of −15 to −10 kcal/mol that exhibit high target affinity (Fig. 4, orange box), such as the cocaine aptamer NC44, which has a K_D of 70 nM and ΔH_{bind} of −10.6 kcal/mol. Although the binding enthalpy makes a small contribution to NC44's affinity relative to other aptamers in the dataset, cocaine binding by NC44 is made much more favorable by the relatively low entropic binding penalty ($T\Delta S_{bind}$ = −0.9 kcal/mol). Given that other cocaine aptamers generally have more negative binding enthalpies and higher entropic penalties, it is possible that binding of NC44 to cocaine may involve hydrophobic interactions. NC44 is unusual, however, in that most of the aptamers with $\Delta H_{bind} \geq -10$ kcal/mol have micromolar K_Ds despite having a low entropic binding penalty ($T\Delta S_{bind} > -2.0$ kcal/mol) (Fig. 4, aquamarine box). This may imply that small-molecule-binding aptamers require a certain threshold of binding enthalpy to achieve high affinity. The aptamer with the lowest binding enthalpy (−3.5 kcal/mol) in our dataset, the AB-FUBINACA aptamer FUB24, binds its target with K_D ~11 μM. Interestingly, it is among the very few aptamers in our dataset with positive binding entropy ($T\Delta S_{bind}$ = +3.2 kcal/mol), which implies that it likely binds its target via hydrophobic interactions. Indeed, positive entropy values were very rare in our dataset, observed in only 3.6% of aptamers. Our data indicate that for most aptamers (~95%), ligand binding is principally an enthalpy-driven process. This is in contrast to protein receptors, for which the binding of small-molecule ligands is often driven either by entropy alone or a combination of enthalpy and entropy [33].

Analyzing the binding thermodynamics of aptamers reported in the literature

We also examined whether the thermodynamic landscape defined here is also more broadly applicable to aptamers discovered by other investigators (Fig. 4, yellow circles). We obtained thermodynamic binding data for previously reported small-molecule-binding DNA aptamers including the dopamine [55] and estradiol [56] aptamers isolated by the Stojanovic group, and the sulforhodamine [57], salicylic acid [58], chloramphenicol [59], adenosine [60], lactate [61], estradiol [62], caffeine [63], and theophylline [64] aptamers isolated by the Liu group. Most of the datapoints corresponding to these aptamers fell within our contour plot, although we observed two outliers. The estradiol aptamer BES.1 isolated by the Stojanovic group exhibits very low binding enthalpy (ΔH_{bind} = −1.9 kcal/mol) and a positive, highly favorable binding entropy ($T\Delta S_{bind}$ = +20.9 kcal/mol) [62]. BES.1 has modest affinity for estradiol (K_D = 1.1 μM), and the thermodynamic data suggest that it most likely binds through hydrophobic interactions. This is supported by the fact that the aptamer, which was derived from an N8 library [56], forms a three-way-junction binding pocket that is commonly associated with a hydrophobic binding mechanism [65]. The other outlier is CN-Es2, another estradiol aptamer isolated by the Liu group [62], which binds its target with ~33-fold higher affinity (K_D = 30 nM) relative to BES.1. This improvement in affinity can be attributed to the ~5-fold more favorable binding enthalpy (ΔH_{bind} = −10.0 kcal/mol) coupled with lower, albeit still favorable, binding entropy ($T\Delta S_{bind}$ = +6.2 kcal/mol). The binding pocket of this aptamer, which was derived from an N30 stem loop DNA library, is likely to be more complex relative to that of BES.1, and may engage in additional forms of non-covalent interaction with estradiol beyond hydrophobic interactions. These outliers are important to consider because they add to the very small number of examples of aptamers that undergo both enthalpy- and entropy-driven ligand binding. Thus, while our thermodynamic dataset appears to broadly describe patterns of binding thermodynamics for aptamers and small-molecule targets, there are clearly other possibilities in thermodynamic space that we have yet to discover.

Examining the relationship between aptamer thermodynamics and specificity

We next asked whether there was any correlation between aptamer-target binding thermodynamics and aptamer specificity. Here, we define specificity as the ability of an aptamer to selectively recognize one target molecule while having minimal affinity for other "interferent" ligands. We have previously employed an exonuclease digestion-based assay [32] to determine the specificity of several of the aptamers in our dataset to a broad variety of ligands. In this assay, aptamers are digested in the absence or presence of ligand by exonuclease I and T5 exonuclease. Unbound aptamers are digested by enzymes into mononucleotides, while ligand-bound aptamers resist enzymatic digestion to an extent that is proportional to the aptamer–ligand binding affinity. Monitoring this digestion process over time using the fluorescent DNA stain SYBR Gold, we can quantify the resistance to enzymatic digestion based on the area under the curve for fluorescence in the absence versus the presence of target. This metric, termed resistance value, serves as a surrogate of aptamer–ligand affinity and can be used to compare the cross-reactivity of an aptamer to a set of ligands. To describe the overall specificity of the aptamer, we have quantified this property with a "specificity score". This is calculated by determining the average cross-reactivity of each aptamer to a given set of interferents, where the number and

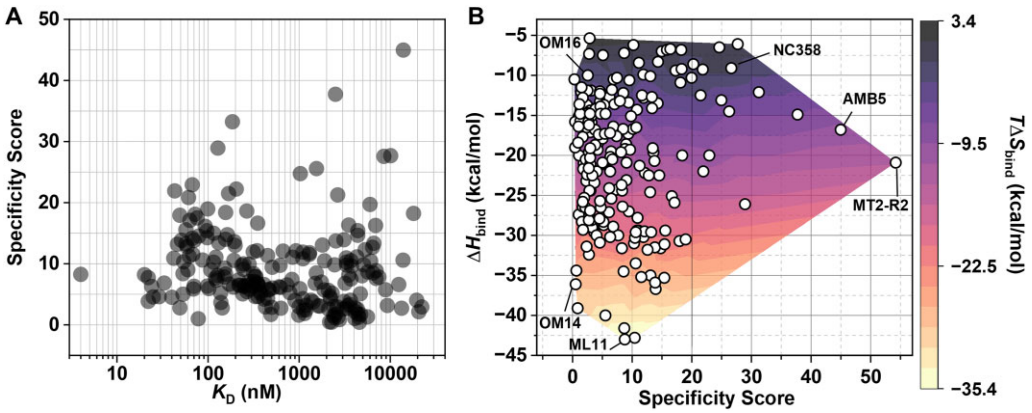

Figure 5. The relationship between aptamer specificity and aptamer–target binding thermodynamics. (**A**) Plot of aptamer target affinity versus specificity score, wherein higher scores indicate poorer affinity. (**B**) A contour plot of specificity scores against enthalpy, with binding entropy as a color gradient. Aptamers discussed in the manuscript are labeled.

identity of the interferents varies for aptamers against different targets. Aptamers with poor specificity have higher specificity scores, and *vice versa*. In our dataset, specificity scores ranged from 0.5 (excellent specificity) to as high as 54 (poor specificity), with an average of 9.3 ± 7.4 and a median of 7.6. We had ~6000 aptamer–ligand pairs in the dataset, yielding 218 unique aptamer specificity scores. We plotted the affinity of each aptamer for its target versus its specificity score to determine if there was a relationship between the two parameters (Fig. 5A), but did not see any correlation. This is in keeping with earlier work from the Szostak group, which characterized a panel of aptamers for guanosine triphosphate and found that high-affinity aptamers did not necessarily have better specificity, leading them to conclude that there is generally no correlation between affinity and specificity [66]. While our data suggest that aptamers with low nanomolar K_D (<50 nM) tend to have good specificity, we remain skeptical as to whether this is really true due to the limited number of datapoints for aptamers in this particular affinity range.

To determine if there was a relationship between binding enthalpy/entropy and specificity, we plotted these values on a two-dimensional contour plot (Fig. 5B). Although we did not see a strong correlation between these parameters, we were able to make some general inferences. First, we noted that there were no aptamers with $\Delta H_{bind} < -35$ kcal/mol and $T\Delta S_{bind} < -25$ kcal/mol that had specificity scores > 15 (our cutoff for good specificity). This led us to hypothesize that aptamers that bind with very high enthalpic contributions and steep entropic penalties are likely to be specific. In other words, if one observes $\Delta H_{bind} < -35$ kcal/mol and $T\Delta S_{bind} < -25$ kcal/mol for aptamer-target binding, it is likely that the aptamer has high specificity. For example, the aptamer with one of the best specificity scores (0.5), OM14 (Supplementary Fig. S13), had a very favorable binding enthalpy of −36 kcal/mol with a large entropy binding penalty ($T\Delta S_{bind} = -28.4$ kcal/mol), while the aptamer with the most negative binding enthalpy and entropy, ML11 ($\Delta H_{bind} = -43$ kcal/mol, $T\Delta S_{bind} = -35.4$ kcal/mol) had a specificity score of 8.9 (Supplementary Fig. S14). ML11 has relatively good specificity, as it cross-reacts to just 5 ligands in a set of 28 interferents, in particular, norepinephrine (25%), amphetamine (25%), dopamine (25%), and quinine (50%). This suggests an intuitively reasonable model in which the more non-covalent interactions form between the aptamer and target (making $\Delta H_{bind} << 0$), and the more the aptamer and/or ligand conformation is restricted ($T\Delta S_{bind} << 0$), the more specific the binding interaction will be. In other words, these enthalpy-driven aptamers achieve high molecular discrimination because they are only capable of interacting with ligands that contain multiple requisite structural features for binding. Our data, however, also indicated that high-specificity binding can be achieved even if enthalpic binding contributions are relatively low. For instance, the oxycodone aptamer OM16 is also specific (specificity score = 2.6) (Supplementary Fig. S15), even though it has much less favorable binding enthalpy (−10 kcal/mol) and entropy ($T\Delta S_{bind} = -2.0$ kcal/mol) compared with OM14. This indicates that specificity can be achieved through other mechanisms, such as high shape complementarity between the aptamer and ligand.

We also observed that as an aptamer's binding enthalpy and entropy become less negative, there is a slight increase in the likelihood of it having poor specificity (Fig. 5B). We made this assessment based on the fact that there are no poorly specific aptamers in our dataset that have $\Delta H_{bind} < -30$ kcal/mol (or $T\Delta S_{bind} < -20$ kcal/mol). For example, cocaine aptamer NC358 has $\Delta H_{bind} = -9.1$ kcal/mol and $T\Delta S_{bind} = 0.1$ kcal/mol, and has the seventh highest specificity score in the dataset. NC358 cross-reacts to ligands with moieties common to cocaine (e.g. amino group and aromatic rings) such as MDPV, mephedrone, MDMA, methadone, heroin, benzoylecgonine, diphenhydramine, procaine, levamisole, fluoxetine, and serotonin (Supplementary Fig. S16). The promiscuity of this aptamer may be due to the presence of a non-specific binding pocket that accommodates ligands with a positive charge and an aromatic moiety. We also observed poor specificity for aptamers that have moderate binding enthalpy and entropy. This is best evidenced by the aptamer with the second poorest specificity (specificity score 45), AMB5, which binds to the hydrophobic synthetic cannabinoid 5F-AMB with a K_D of 13.9 μM, ΔH_{bind} of −16.8 kcal/mol, and $T\Delta S_{bind}$ of −10.2 kcal/mol. This aptamer cross-reacts with a variety of seemingly structurally dissimilar ligands, including lysergic acid diethylamide, quinine, sumatriptan, dehydroepiandrosterone sulfate, procaine, diphenhydramine, oxycodone, MDMA, amphetamine methadone, and cocaine (Supplementary Fig. S17). All of these ligands contain aromatic rings with several hydrogen bond donors and acceptors. Thus, as with NC358, the binding pocket of the aptamer

is able to accommodate a variety of ligands as long as they contain a combination of a few key structural elements. Likewise, the aptamer with the worst specificity score, the methamphetamine aptamer MT2-R2, has moderate binding enthalpy ($\Delta H_{bind} = -20.9$ kcal/ mol) and entropy ($T\Delta S_{bind} = -13.7$ kcal/mol) and cross-reacts to 24 out of 28 tested ligands. Most of these interferents are amines with aromatic rings, including dopamine, serotonin, morphine, methadone, procaine, and diphenhydramine (Supplementary Fig. S18). The data as a whole indicate that the only path toward rationally engineering highly specific aptamers will entail maximizing target-binding enthalpy, binding entropy, or both. This perspective is based on two findings. First, we observed that aptamers with $\Delta H_{bind} > -35$ kcal/mol and $T\Delta S_{bind} > -25$ kcal/mol vary widely in terms of specificity. This indicates that it is challenging to improve aptamer specificity through rational design within this range of thermodynamic parameters. Second, we did not observe any aptamers with $\Delta H_{bind} < -35$ kcal/mol and $T\Delta S_{bind} < -25$ kcal/mol that had a specificity score >15. Thus, the data suggest that pushing ΔH_{bind} and $T\Delta S_{bind}$ below −35 and −25 kcal/mol, respectively, represents a rational path toward high specificity. However, because there are only a handful of datapoints in this part of the thermodynamic space, it is possible that our assumptions may need to be modified in light of future data.

Discussion

Here, we have compiled and analyzed thermodynamic binding data derived from ITC as well as specificity data from an exonuclease digestion assay for a panel of >300 DNA aptamers for small-molecule targets. In general, we observed close correlation between ΔH_{bind} and ΔS_{bind}, similar to what previous biophysical studies have found with protein–ligand interactions [33], but saw no meaningful correlation between aptamer affinity and ΔH_{bind} or ΔS_{bind}. For instance, there were several high-affinity aptamers ($K_D < 100$ nM) with a broad range of binding enthalpy (−40 to −10 kcal/mol) and entropy values (−30 to 0 kcal/mol). This implies that high-affinity recognition of small-molecule targets by aptamers can be achieved through a variety of interaction mechanisms. By creating contour plots from the binding enthalpy, entropy, and affinity data, we were able to make some general observations. For example, the highest-affinity aptamers had neither the most negative binding enthalpy nor the most positive binding entropy, and aptamers with the highest binding enthalpy tended to have lower binding affinity. Finally, we determined that although there is poor correlation between aptamer specificity and target-binding enthalpy and entropy, the likelihood of an aptamer having poor specificity decreases as its binding enthalpy and entropy become increasingly negative. Compared with the thermodynamics of protein binding to small molecules, which is primarily driven either by entropy alone or by both entropy and enthalpy, our dataset indicates that the thermodynamics of aptamer–small molecule binding are, surprisingly, predominately driven by enthalpy, with both entropy- and enthalpy-driven binding apparent only in a minority of aptamers. Despite initial concerns that our dataset may have been biased toward enthalpy-driven binding due to the collection of measurements with ITC, which detects binding events by measuring heats of binding reactions, we subsequently recognized that ITC should be capable of detecting entropy-driven binding ($T\Delta S_{bind} > 0$ kcal/mol) because ΔH_{bind} would be ≥ 0 kcal/mol (i.e. endothermic binding) in such cases. We do acknowledge, however, that ITC will face difficulties accurately quantifying binding thermodynamics if ΔH_{bind} is between −2.0 and +2.0 kcal/mol due to low signal-to-noise ratios. Alternative affinity determination methods, such as microscale thermophoresis, would thus be more appropriate in such cases.

Our study has several limitations that should be considered. First, the small-molecule ligands in our dataset are either drugs or drug-like molecules that follow Lipinski's "Rule of 5" [67], and thus tend to be hydrophobic rather than hydrophilic, with an average LogP of 2.9. However, there are several aptamers that bind to hydrophilic targets including amino acids, carbohydrates, and nucleotides, which are underrepresented in our dataset. Nevertheless, our data here can be consolidated with thermodynamic data obtained for these more hydrophilic ligands in the future. Second, we would like to caution readers that, because there are likely more aptamers for our ligands that we have not yet discovered, the conclusions that we have drawn here from the thermodynamic data apply to the aptamers we have discovered thus far. In any case, however, if in the future more aptamers are discovered for the ligands studied in this work, the new thermodynamic data can be integrated into the dataset provided here to make more generalizable conclusions. Third, it remains unclear to what extent the binding thermodynamics of aptamer–small molecule binding is comparable to binding between aptamers and protein targets. In particular, protein-binding aptamers undergo unique binding phenomena that may not be observed with small-molecule-binding aptamers, such as the displacement of counterions in the ionic milieu of nucleic acids and proteins upon nucleic acid–protein binding [68]. Since this process is entropically favorable, the binding thermodynamics for some protein-binding aptamers will differ from those of small molecule–aptamer binding—which, as we find here, are generally enthalpy-driven and entropically unfavorable. Fourth, since our aptamers are all based on DNA, the generalizability of our findings to RNA aptamers is currently unknown. Finally, we would like to note that the specificity score we used in this work is merely an estimate of aptamer specificity. This is because these scores were derived from cross-reactivity values determined via exonuclease digestion assays with just one concentration of interferent. Perhaps a more suitable metric for specificity is the actual measured affinity of an aptamer for interferents in terms of K_D, as obtained via ITC or strand-displacement assays. Obtaining such data, however, will require considerable effort and time, as most methods for determining K_D have low throughput. Nevertheless, the findings here will serve as a foundation for broader exploration of the parameters that more generally inform aptamer binding behavior in the future.

Acknowledgements

Author contributions: O.A. was involved in data collection and analysis, methodology, software, data validation, and original draft preparation and writing. J.C., C.B., A.B., and R.H. contributed to data collection and analysis and paper reviewing and editing. Y.X. was involved in project administration, conceptualization, data analysis, writing, and funding acquisition.

Supplementary data

Supplementary data is available at NAR online.

Conflict of interest

The authors declare no competing financial interest.

Funding

This work was supported by the National Institute of Justice, Office of Justice Programs award 2022-GG-04440-RESS. Funding to pay the Open Access publication charges for this article was provided by National Institute of Justice award 2022-GG-04440-RESS.

Data availability

The ITC and binding data underlying this article are available in the article and in its online supplementary material.

References

1. Tuerk C, Gold L. Systematic evolution of ligands by exponential enrichment: RNA ligands to bacteriophage T4 DNA polymerase. *Science* 1990;**249**:1465–8. https://doi.org/10.1126/science.2200121
2. Ellington AD, Szostak JW. *In vitro* selection of RNA molecules that bind specific ligands. *Nature* 1990;**346**:818–22. https://doi.org/10.1038/346818a0
3. Dunn MR, Jimenez RM, Chaput JC. Analysis of aptamer discovery and technology. *Nat Rev Chem* 2017;**1**:0076. https://doi.org/10.1038/s41570-017-0076
4. Zhou J, Rossi J. Aptamers as targeted therapeutics: current potential and challenges. *Nat Rev Drug Discov* 2017;**16**:181–202. https://doi.org/10.1038/nrd.2016.199
5. Downs AM, Plaxco KW. Real-time, *in vivo* molecular monitoring using electrochemical aptamer based sensors: opportunities and challenges. *ACS Sens* 2022;**7**:2823–32. https://doi.org/10.1021/acssensors.2c01428
6. Yu H, Frederiksen J, Sullenger BA. Aptamer-based protein inhibitors. In: *RNA Therapeutics: The Evolving Landscape of RNA Therapeutics*. Academic Press, 2022, 89–120.
7. He J, Duan Q, Ran C *et al.* Recent progress of aptamer–drug conjugates in cancer therapy. *Acta Pharm Sin B* 2023;**13**:1358–70. https://doi.org/10.1016/j.apsb.2023.01.017
8. Hermann T, Patel DJ. Adaptive recognition by nucleic acid aptamers. *Science* 2000;**287**:820–5. https://doi.org/10.1126/science.287.5454.820
9. Xu G, Zhao J, Liu N *et al.* Structure-guided post-SELEX optimization of an ochratoxin A aptamer. *Nucleic Acids Res* 2019;**47**:5963–72. https://doi.org/10.1093/nar/gkz336
10. Xu G, Zhao J, Yu H *et al.* Structural insights into the mechanism of high-affinity binding of ochratoxin A by a DNA aptamer. *J Am Chem Soc* 2022;**144**:7731–40. https://doi.org/10.1021/jacs.2c00478
11. Lin CH, Patel DJ. Structural basis of DNA folding and recognition in an AMP–DNA aptamer complex: distinct architectures but common recognition motifs for DNA and RNA aptamers complexed to AMP. *Chem Biol* 1997;**4**:817–32. https://doi.org/10.1016/S1074-5521(97)90115-0
12. Ren A, Rajashankar KR, Patel DJ. Fluoride ion encapsulation by Mg^{2+} ions and phosphates in a fluoride riboswitch. *Nature* 2012;**486**:85–9. https://doi.org/10.1038/nature11152
13. Passalacqua LFM, Banco MT, Moon JD *et al.* Intricate 3D architecture of a DNA mimic of GFP. *Nature* 2023;**618**:1078–84. https://doi.org/10.1038/s41586-023-06229-8
14. Slavkovic S, Johnson PE. Analysis of aptamer–small molecule binding interactions using isothermal titration calorimetry. In: Mayer G, Menger MM (eds.), *Nucleic Acid Aptamers – Selection, Characterization, and Application*. Humana, New York, NY: Springer, 2023, 105–18.
15. Prabhu NV, Sharp KA. Heat capacity in proteins. *Annu Rev Phys Chem* 2005;**56**:521–48. https://doi.org/10.1146/annurev.physchem.56.092503.141202
16. Eisen SR, Dauphin-Ducharme P, Johnson PE. Solution-based biophysical characterization of conformation change in structure-switching aptamers. *Q Rev Biophys* 2024;**57**:e9. https://doi.org/10.1017/S0033583524000076
17. Chang AL, McKeague M, Smolke CD. Facile characterization of aptamer kinetic and equilibrium binding properties using surface plasmon resonance. *Methods Enzymol* 2014;**549**:451–66. https://doi.org/10.1016/B978-0-12-801122-5.00019-2
18. Yang KA, Chun H, Zhang Y *et al.* High-affinity nucleic-acid-based receptors for steroids. *ACS Chem Biol* 2017;**12**:3103–12. https://doi.org/10.1021/acschembio.7b00634
19. Slavkovic S, Churcher ZR, Johnson PE. Nanomolar binding affinity of quinine-based antimalarial compounds by the cocaine-binding aptamer. *Bioorg Med Chem* 2018;**26**:5427–34. https://doi.org/10.1016/j.bmc.2018.09.017
20. Ding Y, Liu X, Huang PJJ *et al.* Homogeneous assays for aptamer-based ethanolamine sensing: no indication of target binding. *Analyst* 2022;**147**:1348–56. https://doi.org/10.1039/D2AN00145D
21. Liu X, Hou Y, Chen S *et al.* Controlling dopamine binding by the new aptamer for a FRET-based biosensor. *Biosens Bioelectron* 2021;**173**:112798. https://doi.org/10.1016/j.bios.2020.112798
22. Slavkovic S, Eisen SR, Johnson PE. Designed alteration of binding affinity in structure-switching aptamers through the use of dangling nucleotides. *Biochemistry* 2020;**59**:663–70. https://doi.org/10.1021/acs.biochem.9b00630
23. Neves MAD, Reinstein O, Johnson PE. Defining a stem length-dependent binding mechanism for the cocaine-binding aptamer. A combined NMR and calorimetry study. *Biochemistry* 2010;**49**:8478–87. https://doi.org/10.1021/bi100952k
24. Neves MAD, Reinstein O, Saad M *et al.* Defining the secondary structural requirements of a cocaine-binding aptamer by a thermodynamic and mutation study. *Biophys Chem* 2010;**153**:9–16. https://doi.org/10.1016/j.bpc.2010.09.009
25. Canoura J, Yu H, Alkhamis O *et al.* Accelerating post-SELEX aptamer engineering using exonuclease digestion. *J Am Chem Soc* 2021;**143**:805–16. https://doi.org/10.1021/jacs.0c09559
26. Samokhvalov AV, Safenkova IV, Eremin SA *et al.* Modulation of aptamer–ligand-binding by complementary oligonucleotides: a G-quadruplex anti-ochratoxin A aptamer case study. *Int J Mol Sci* 2022;**23**:4876. https://doi.org/10.3390/ijms23094876
27. Dawood NE, Slavkovic S, Qureshi R *et al.* Cooperative binding by a bifunctional deoxycholic acid and cocaine-binding aptamer. *Aptamers* 2021;**5**:31–8.
28. McKeague M, McConnell EM, Cruz-Toledo J *et al.* Analysis of *in vitro* aptamer selection parameters. *J Mol Evol* 2015;**81**:150–61. https://doi.org/10.1007/s00239-015-9708-6
29. Drees A, Trinh TL, Fischer M. The influence of protein charge and molecular weight on the affinity of aptamers. *Pharmaceuticals* 2023;**16**:457. https://doi.org/10.3390/ph16030457
30. Sakamoto T, Ennifar E, Nakamura Y. Thermodynamic study of aptamers binding to their target proteins. *Biochimie* 2018;**145**:91–7. https://doi.org/10.1016/j.biochi.2017.10.010
31. Slavkovic S, Altunisik M, Reinstein O *et al.* Structure–affinity relationship of the cocaine-binding aptamer with quinine derivatives. *Bioorg Med Chem* 2015;**23**:2593–7. https://doi.org/10.1016/j.bmc.2015.02.052

32. Alkhamis O, Yang W, Farhana R *et al.* Label-free profiling of DNA aptamer–small molecule binding using T5 exonuclease. *Nucleic Acids Res* 2020;**48**:e120. https://doi.org/10.1093/nar/gkaa849
33. Gilli P, Ferretti V, Gilli G *et al.* Enthalpy–entropy compensation in drug–receptor binding. *J Phys Chem* 1994;**98**:1515–8. https://doi.org/10.1021/j100056a024
34. Olsson TSG, Williams MA, Pitt WR *et al.* The thermodynamics of protein–ligand interaction and solvation: insights for ligand design. *J Mol Biol* 2008;**384**:1002–17. https://doi.org/10.1016/j.jmb.2008.09.073
35. Canoura J, Alkhamis O, Liu Y *et al.* High-throughput quantitative binding analysis of DNA aptamers using exonucleases. *Nucleic Acids Res* 2023;**51**:e19. https://doi.org/10.1093/nar/gkac1210
36. Yang W, Yu H, Alkhamis O *et al.* *In vitro* isolation of class-specific oligonucleotide-based small-molecule receptors. *Nucleic Acids Res* 2019;**47**:e71. https://doi.org/10.1093/nar/gkz224
37. Yu H, Luo Y, Alkhamis O *et al.* Isolation of natural DNA aptamers for challenging small-molecule targets, cannabinoids. *Anal Chem* 2021;**93**:3172–80. https://doi.org/10.1021/acs.analchem.0c04592
38. Alkhamis O, Xiao Y. Systematic study of *in vitro* selection stringency reveals how to enrich high-affinity aptamers. *J Am Chem Soc* 2023;**145**:194–206. https://doi.org/10.1021/jacs.2c09522
39. Alkhamis O, Canoura J, Wang L *et al.* Nuclease-assisted selection of slow-off rate aptamers. *Sci Adv* 2024;**10**:eadl3426. https://doi.org/10.1126/sciadv.adl3426
40. Alkhamis O, Canoura J, Wu Y *et al.* High-affinity aptamers for *in vitro* and *in vivo* cocaine sensing. *J Am Chem Soc* 2024;**146**:3230–40. https://doi.org/10.1021/jacs.3c11350
41. Wang L, Canoura J, Byrd C *et al.* Examining the relationship between aptamer complexity and molecular discrimination of a low-epitope target. *ACS Cent Sci* 2024;**10**:2213–28. https://doi.org/10.1021/acscentsci.4c01377
42. Canoura J, Nguyen T, Byrd C *et al.* Generation of high-affinity aptamers for indazole synthetic cannabinoids. *Anal Chem* 2024;**96**:11488–97. https://doi.org/10.1021/acs.analchem.4c02151
43. Canoura J, Alkhamis O, Venzke M *et al.* Developing aptamer-based colorimetric opioid tests. *JACS Au* 2024;**4**:1059–72. https://doi.org/10.1021/jacsau.3c00801
44. Canoura J, Liu Y, Alkhamis O *et al.* Aptamer-based fentanyl detection in biological fluids. *Anal Chem* 2023;**95**:18258–67. https://doi.org/10.1021/acs.analchem.3c04104
45. Wang L, Alkhamis O, Canoura J *et al.* Rapid nuclease-assisted selection of high-affinity small-molecule aptamers. *J Am Chem Soc* 2024;**146**:21296–307. https://doi.org/10.1021/jacs.4c00748
46. Yu H, Canoura J, Byrd C *et al.* Improving aptamer affinity and determining sequence–activity relationships via Motif–SELEX. *J Am Chem Soc* 2024;**147**:9472–86. https://doi.org/10.1021/jacs.4c17041
47. Canoura J, Alkhamis O, Byrd C *et al.* Determining the precision of high throughput sequence and its influence on aptamer selection. *Anal Chem* 2024;**96**:17720–9. https://doi.org/10.1021/acs.analchem.4c03972
48. Zadeh JN, Steenberg CD, Bois JS *et al.* NUPACK: analysis and design of nucleic acid systems. *J Comput Chem* 2011;**32**:170–3. https://doi.org/10.1002/jcc.21596
49. Zuker M. Mfold web server for nucleic acid folding and hybridization prediction. *Nucleic Acids Res* 2003;**31**:3406–15. https://doi.org/10.1093/nar/gkg595
50. Volpe DA, Tobin GAMM, Mellon RD *et al.* Uniform assessment and ranking of opioid Mu receptor binding constants for selected opioid drugs. *Regul Toxicol Pharmacol* 2011;**59**:385–90. https://doi.org/10.1016/j.yrtph.2010.12.007
51. Yang K, Mitchell NM, Banerjee S *et al.* A functional group-guided approach to aptamers for small molecules. *Science* 2023;**380**:942–8. https://doi.org/10.1126/science.abn9859
52. Sharp K. Entropy–enthalpy compensation: fact or artifact? *Protein Sci* 2001;**10**:661–7. https://doi.org/10.1110/ps.37801
53. Chodera JD, Mobley DL. Entropy–enthalpy compensation: role and ramifications in biomolecular ligand recognition and design. *Annu Rev Biophys* 2013;**42**:121–42. https://doi.org/10.1146/annurev-biophys-083012-130318
54. Yang K, Alkhamis O, Canoura J *et al.* Exploring the landscape of aptamers: from cross-reactive to selective to specific, high-affinity receptors for cocaine. *JACS Au* 2024;**4**:760–70. https://doi.org/10.1021/jacsau.3c00781
55. Nakatsuka N, Yang K-A, Abendroth JM *et al.* Aptamer–field-effect transistors overcome Debye length limitations for small-molecule sensing. *Science* 2018;**362**:319–24. https://doi.org/10.1126/science.aao6750
56. Yang K-A, Pei R, Stefanovic D *et al.* Optimizing cross-reactivity with evolutionary search for sensors. *J Am Chem Soc* 2012;**134**:1642–7. https://doi.org/10.1021/ja2084256
57. Gu L, Zheng J, Zhang Y *et al.* Capture–SELEX of DNA aptamers for sulforhodamine B and fluorescein. *Chemistry* 2023;**29**:e202302616. https://doi.org/10.1002/chem.202302616
58. Gu L, Zhang H, Ding Y *et al.* Capture–SELEX for a short aptamer for label-free detection of salicylic acid. *Smart Mol* 2023;**1**:e20230007. https://doi.org/10.1002/smo.20230007
59. Zhao Y, Li AZ, Liu J. Capture–SELEX for chloramphenicol binding aptamers for labeled and label-free fluorescence sensing. *Environ Health* 2023;**1**:102–9. https://doi.org/10.1021/envhealth.3c00017
60. Ding Y, Liu J. Pushing adenosine and ATP SELEX for DNA aptamers with nanomolar affinity. *J Am Chem Soc* 2023;**145**:7540–7. https://doi.org/10.1021/jacs.3c00848
61. Huang PJJ, Liu J. Simultaneous detection of L-lactate and D-glucose using DNA aptamers in human blood serum. *Angew Chem Int Ed* 2023;**62**:e202212879. https://doi.org/10.1002/anie.202212879
62. Niu C, Zhang C, Liu J. Capture–SELEX of DNA aptamers for estradiol specifically and estrogenic compounds collectively. *Environ Sci Technol* 2022;**56**:17702–11. https://doi.org/10.1021/acs.est.2c05808
63. Huang PJJ, Liu J. Selection of aptamers for sensing caffeine and discrimination of its three single demethylated analogues. *Anal Chem* 2022;**94**:3142–9. https://doi.org/10.1021/acs.analchem.1c04349
64. Huang PJJ, Liu J. A DNA aptamer for theophylline with ultrahigh selectivity reminiscent of the classic RNA aptamer. *ACS Chem Biol* 2022;**17**:2121–9. https://doi.org/10.1021/acschembio.2c00179
65. Kato T, Yano K, Ikebukuro K *et al.* Interaction of three-way DNA junctions with steroids. *Nucleic Acids Res* 2000;**28**:1963–8. https://doi.org/10.1093/nar/28.9.1963
66. Carothers JM, Oestreich SC, Szostak JW. Aptamers selected for higher-affinity binding are not more specific for the target ligand. *J Am Chem Soc* 2006;**128**:7929–37. https://doi.org/10.1021/ja060952q
67. Lipinski CA, Lombardo F, Dominy BW *et al.* Experimental and computational approaches to estimate solubility and permeability in drug discovery and drug development settings. *Adv Drug Delivery Rev* 1997;**23**:3–25. https://doi.org/10.1016/S0169-409X(96)00423-1
68. Pletka CC, Nepravishta R, Iwahara J. Detecting counterion dynamics in DNA–protein association. *Angew Chem Int Ed* 2020;**59**:1465–8. https://doi.org/10.1002/anie.201910960

Received: November 30, 2024. **Revised:** February 18, 2025. **Editorial Decision:** March 4, 2025. **Accepted:** March 11, 2025